LAWRENCE
LIVERMORE
NATIONAL
LABORATORY

LLNL-JRNL-648158

The plutonium-hydrogen reaction: SEM characterization of product morphology

L. N. Dinh, S. K. McCall, C. K. Saw, J. M. Haschke, P. G. Allen, W. McClean II

December 31, 2013

Journal of Nuclear Materials

Disclaimer

The plutonium-hydrogen reaction: SEM characterization of product morphology

L.N. Dinh*, S. K. McCall, C. K. Saw, J. M. Haschke, P. G. Allen, W. McLean II

Lawrence Livermore National Laboratory, Livermore, CA 94551, USA

*Corresponding author. Address: Lawrence Livermore National Laboratory, 7000 East Avenue, Mail Stop: L-091, Livermore, CA 94551, USA. Tel.: +1 925 422 4271. E-mail address: Dinh1@llnl.gov (L. N. Dinh).

Abstract

The product morphology of the hydrogen reaction with plutonium near the visibly observable reaction front, which separates the hydrided zone from the unreacted metal zone, has been investigated by scanning electron microscopy (SEM). Results indicate the existence of a mixed phase of metal and metal hydride, located some 20-30 μm ahead of the visibly hydrided-zone. The mixed phase regions are often located next to a grain boundary network and exhibit rays of hydride advancing toward the unreacted metal regions. Analysis indicates that hydrogen transport and therefore the hydriding reaction are preferable along the grain boundary network and defects in the metal structure rather than through a homogeneous intragrain reaction. Product fracture and formation of small hydride particles during hydriding are likely results of such inhomogeneous growth.

Introduction

Plutonium hydriding is a rapid corrosion reaction that produces both dispersible and respirable plutonium-containing particles [1]. Plutonium hydride (PuH_x, $2 \leq x \leq 3$) is

pyrophoric and known to catalyze violent reactions with both oxygen and nitrogen upon air exposure [1]. Therefore, an in-depth knowledge of plutonium hydriding is of technical interest and has practical consequences in the protection of personnel and the environment during handling, transport, and storage of Pu.

The process of plutonium hydriding usually involves an induction time, an often difficult to predict period during which Pu is exposed to H_2 without any detectable sign of hydriding and is usually attributed to the slow diffusion of hydrogen through the PuO_2 surface layer protecting the underlying Pu metal [2-6]. The induction period ends with an observable nucleation site which rapidly reacts with hydrogen and grows in size. During the growth of this original site, other initiation sites may spontaneously appear and coalesce. The hydriding process continues until either hydrogen or plutonium is exhausted. Such a multi-stage hydriding process has been reported [2, 7-11]. Based on thermodynamics and experimental data, it has been argued that hydrogen transport through the PuO_2 protection layer is supported mainly through grain boundaries, cracks, oxygen vacancies, Pu_2O_3 [8, 12] domains, and other defects in the dioxide structure. A separate report, combining pyrometric experiments and thermal modeling suggests that hydrogen transport along grain boundaries in the Pu metal structure is faster than intragrain reaction [9].

In this article, the morphology of the product of hydrogen reaction with plutonium near the boundary between the visibly hydrided region and the unreacted metal is reported. The implications of the SEM analysis on the preferred hydrogen transport routes, hydriding growth mode, and their effects on hydride product will also be discussed.

Experiments

Hydriding experiments were made in an argon-atmosphere glove box using circular (16 mm diameter) coupons cut from a 0.8 mm thick sheet of Ga stabilized δ-Pu. The samples were rinsed with ethanol to remove machining residues and dried in an argon glovebox before testing. The thickness of the PuO_2 surface layer was determined to be about 220 nm by ion milling and SEM. During a typical hydriding experiment, the test specimen was mounted in a two-piece aluminum holder fitted with a pair of indium o-ring seals pressed against the perimeter of the Pu sample surface. Access of H_2 to the Pu sample during the initial phase of the hydriding process was confined to the visually observable 13mm diameter opening in the front aluminum plate. As the hydriding experiments progressed, eventually a corrosion hole formed allowing rapid transport of H_2 to the unobservable back of the sample, where reactions akin to the front surface began. The mounted sample was placed in an evacuable stainless steel reaction chamber equipped with a turbomolecular pump, type K thermocouples, calibrated capacitance manometers (MKS), and sapphire windows for viewing/imaging.

For the SEM work, hydriding experiments were stopped early resulting in partial hydriding of the sample, and then exposed to oxygen to convert the pyrophoric hydride to oxide. The samples were subsequently potted in epoxy (Allied EpoxyMount Resin), and polished with 1200 grit sandpaper. The final polish was done with 1 micron diamond grit and finished with 0.25 micron diamond grit on microcloth, both under kerosene. The sample was taped off with carbon tape to limit charging effects. Imaging was performed using an FEI Quanta 3D FEG scanning electron microscope. A 50 micron square box was milled approximately 1 micron deep with a Ga beam at 8 KV and 0.24 nA to expose sample features such as grain boundaries (average grain size of ~ 40 microns). The low energy settings were used to limit loose contamination within the instrument. Areas of interest within the milled area were identified for

cross-sectioning and high resolution imaging. The standard recipe for this high resolution imaging procedure was to deposit a 5 micron layer of Pt with an electron beam at a 0° tilt to protect the area from FIB deformation. After deposition, the sample was tilted to 52° and a second Pt deposition of 5 microns was performed with the FIB. A rough cross section was then constructed, typically 10 microns wide, by 7 microns deep, and 21 microns in length, using a Ga beam at 8 KV and 0.24 nA. Finally, a brief cleaning cross-section at 30 KV and 3 nA provided a final polish and sharply reduced the observed curtaining effect. The cross-sections were imaged at 10 KV at an angle of 52-54° and are called off-axis FIB-SEM in this report. Microprobe measurements were performed with a JEOL 733 Superprobe using secondary electron imaging at 15 KV and 20 nA to map the Fe distribution on the sample surface.

Results and discussion

The geometry of hydrogen corrosion growth in polycrystalline δ-Pu is three dimensional (3D) as illustrated in the SEM images of a cross section of a partially hydrided sample shown in Fig. 1. Since the density of the hydride is ~ 60% that of δ-Pu, hydrided regions tend to break up to release stress and appear darker in SEM images. Sites labeled with "A1" and "A2" were formed mostly by isolated hydride spots, while site "B" was formed by the merging of nearby initiation sites. When nearby initiation sites merge, the coalesced hydride spot tends to have a rough reaction front and becomes oblate. In contrast, isolated initiation sites like those labeled "A1" in Fig. 3(a) tend to grow hemispherically. However, there are isolated hydride spots that advance more ellipsoidally with the ratio of major axis to minor axis as high as 2 (site A2). More detailed morphologies are explored in the next section for three locations identified in Fig.

3(c): 1) at the reaction front; 2) along a grain boundary located ~ 20 to 30 μm from the reaction front; and 3) in the unreacted metal region far away from the reaction front.

Fig. 2(a) illustrates the technique of off-axis FIB-SEM imaging employed in this work, where two FIB cross-sections of the macroscopically cross-sectioned sample are shown. FIB-SEM images of the reaction front (location 1 in Fig. 1(c)) are shown in Fig. 2(b-d). Higher magnification imaging reveals the existence of cracks in the hydrided area [Fig. 2(c)] and a mixture of Pu (brighter areas) and PuH_x (darker areas) near the reaction front [Fig. 2(d)]. Due to the great difference in densities between the Pu alloy (~16.0 g/cm^3) and PuH_x (~10.4 g/cm^3), it is logical to expect cracks to develop during the hydriding process. The experimental observation of a mixed Pu + PuH_x phase near the reaction front, which is conventionally defined as the boundary between the hydrided region and the unreacted metal, is reported for the first time here.

In Fig. 3, a FIB-SEM image at a grain boundary some 20 to 30 μm ahead of the apparent reaction front is presented (same as location 2 in Fig. 1(c)). Microprobe measurements show that the lighter phase in the grain boundary is Pu_6Fe, which is an intermetallic compound formed by iron impurities often segregated at grain boundaries. Higher magnification in Fig. 3(b) reveals partial hydriding of the grain adjacent to Pu_6Fe at this grain boundary location. Indeed, a receding gradient of hydride can be seen running from the grain boundary to the inner portion of this grain. The existence of partially hydrided grains some 20 to 30 μm ahead of the visibly observable hydrided region qualitatively confirms that hydrogen transport along grain boundaries is faster than the intragrain reaction as previously deduced from a comparison between thermal modeling and experiments combining pyrometric imaging with pressure drop measurement [9].

Images obtained at another hydriding spot [Fig. 4] exhibit the existence of two observable reaction fronts. In Fig. 4(a), the two dashed lines labeled R1 and R2 indicate the extents of hydrided and partially hydrided regions, respectively. From the higher magnification image (Fig 4(b)) of the boundary between the fully and partially hydrided regions of the reaction front, it is seen that the reaction front did not advance uniformly but as spikes of hydride (rays of darker lines). Point dislocations formed by self-irradiation from Pu-239 decay can coalesce into lines or spiral dislocations within the metal grains [13-15]. Dislocations, localized alpha-phase regions [16] and other anomalies in the grains are likely easier pathways for the observed non-uniform penetration of hydride. So, the faster route for hydrogen transport is most likely not only along the grain boundary network, but also through cracks and anomalies/defects in the Pu metal structure, in qualitative agreement with prior work [9]. This inhomogeneous hydriding growth most likely leads to product fractures during reaction and formation of small hydride particles.

However, a few grains ahead of the reaction front, no visible hydriding was observed as shown in Fig. 5. The reason for the speckling seen on the right grain and its absence on the left grain in the image is unknown, but may be an artifact of the FIB along particular crystallographic orientations of the Pu. Perhaps, some defects such as dislocations may form more favorably along certain crystallographic orientation than others. But sectioning through hydride spikes formed along dislocations normal to the viewing plane might produce an array of spots like those observed in the right grain. Note that the faint square and rectangular marks in the SEM image are artifacts due to previous electron beam exposure over those areas.

Conclusions

SEM characterization reveals the existence of a partially hydrided zone containing a mixed phase of metal and metal hydride, extending some 20-30 μm ahead of the visible hydrided zone. These partially hydrided regions are often observed adjacent to a grain boundary network and as rays of hydride piercing through, probably, defects in the unreacted metal such as cracks, localized alpha phase, or line dislocations. The results of this SEM investigation qualitatively confirm that hydrogen transport and therefore reaction are preferable along the grain boundary network and defects/anomalies in the metal structure rather than through a homogeneous intragrain reaction. This inhomogeneous hydriding growth, coupled with the great density differences between the unreacted metal and hydride, expectedly leads to product fracture and formation of small hydride particles as often seen with plutonium hydriding.

Acknowledgement

We would like to acknowledge the expertise of Robert Erler for the SEM work, the technical assistance of Rory Gollott in Pu handling, and the many illuminating discussions with Dr. W. J. Siekhaus on the subject of actinide hydriding. This work was performed under the auspices of the U.S. Department of Energy by Lawrence Livermore National Laboratory under Contract DE-AC52-07NA27344.

References

[1] J. M. Haschke, J. L. Stakebake, in The Chemistry of the Actinide and Transuranium Elements, vol. 5, L. R. Morss, N. M. Edelstein, J. Fuger, Springer, 2006, pp. 3199-3272.

[2] G.W. McGillivray, J.P. Knowles, I.M. Findlay, M.J. Dawes, J. Nucl. Mater. **412** (2011) 35-40.

[3] J. Bloch, E. Swissa, M. H. Mintz, Z. Phys. Chem. Neue Folge, **1964** (1989) 1193.

[4] J. Bloch, M. H. Mintz, L. Less Common Met. **166** (1990) 241.

[5] D. Cohen, Y. Zeiri, M. H. Mintz, J. Alloys Compd. **184** (1992) 11.

[6] J. Glasscott, AWE Discovery **6** (2003) 6.

[7] J. M. Haschke, Synthesis of Lanthanide and Actinide Compounds, edited by G. Meyer, L. R. Morss, Kluwer Academic Publishers (2001), p. 1-53.

[8] L.N. Dinh, J.M. Haschke, C.K. Saw, P.G. Allen, W. McLean II, J. Nucl. Mater. **408** (2011) 171-175.

[9] C. K. Saw, J. M. Haschke, P. G. Allen, W. McLean II, L. N. Dinh, J. Nucl. Mater. **429**, (2012) 128-135.

[10] G. W. McGillivray, J. P. Knowles, I. M. Findlay, M. J. Dawes, J. Nucl. Mater. **385** (2009), 212-215.

[11] K. Balasubramanian, T. E. Felter, T. Anklam, T. W. Trelenberg, W. McLean II, J. Alloys Compds. **444-445** (2007) 447-452.

[12] J.M. Haschke, T.J. Allen, and L.A. Morales, Los Alamos Science, **26** (2000) 253-273.

[13] Y. Hiki, T. Kosugi, K. Mijuno, T. Kino, Solute Atom-Dislocation Interactions studied by Ultrasonic Method, in Points Defects and Defect interactions in Metals, J. –I. Takamura, M. Doyama, M, Kiritani, North-Holland Publishing Co., Amsterdam, 1982, p. 753-755.

[14] Y. Shimomura, K. Kitagawa, Y. Takai, H. Hashimoto, High Resolution Electron Microscopy Observation of Small Point Defect Clusters and Their Thermal Stability, in Points Defects and Defect interactions in Metals, J. –I. Takamura, M. Doyama, M, Kiritani, North-Holland Publishing Co., Amsterdam, 1982, p. 708-711.

[15] H. E. Flotow, J. M. Haschke, S. Yamauchi, The Chemical Thermodynamics of Actinide Elements and Compounds, part 9, F. L. Oetting, Ed., International Atomic Energy Agency, Vienna, 1984.

[16] K. J. M. Blobaum, C. R. Krenn, M. A. Wall, T. B. Massalski, A. J. Schwartz, Acta Materialia **54** (2006) 4001.

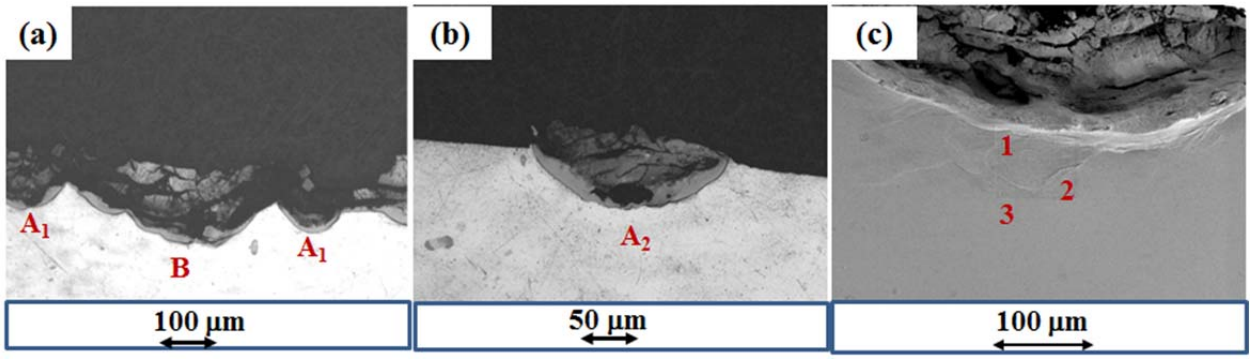

Fig. (1): The geometries of hydrogen corrosion in polycrystalline δ-Pu. SEM images in (a) and (b) suggest that "A1" and "A2" were primarily formed by isolated initiation sites, while "B" formed through the merging of nearby initiation sites. More detailed morphologies at the reaction front (1), along a grain boundary some 20 to 30 µm away from the reaction front, and (3) well inside the unreacted metal as labeled in (c) are explored in subsequent figures.

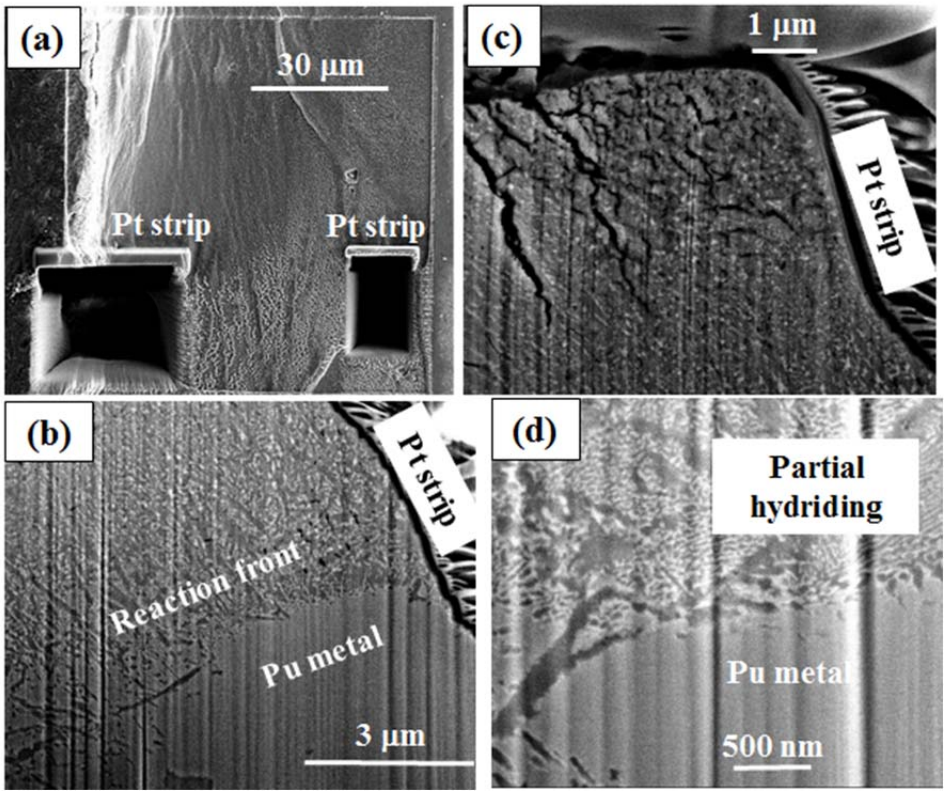

Fig. (2): (a) cross sectional SEM images are taken from the left trench looking at the upper wall cutting across the corrosion front. Image (b) shows the reaction front as a mixture of Pu (bright areas) and PuH_x (darker areas). Image (c) reveals the existence of cracking in the hydrided area while (d) shows a higher magnification image of the reaction front. The sputtered Pt strap used to protect the surface while cross sectioning is visible in (a) (b) and (c).

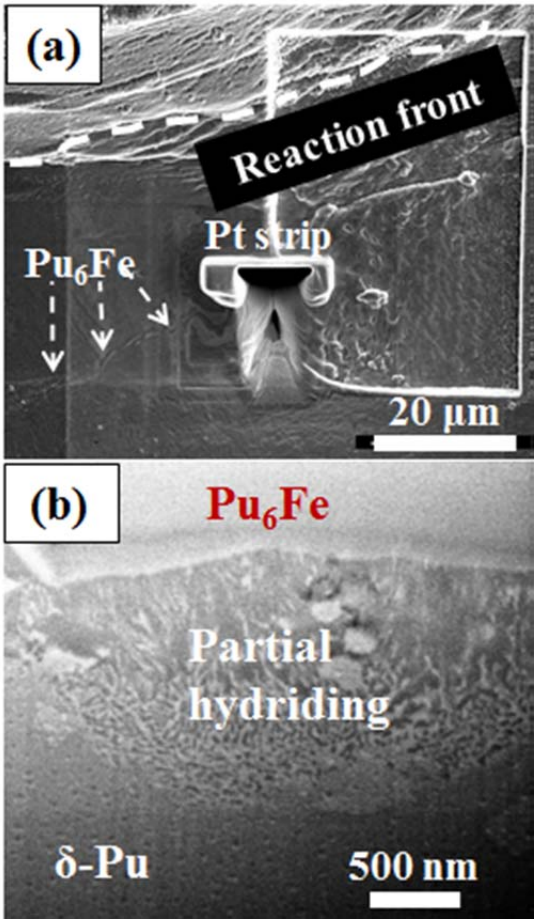

Fig. (3): (a) SEM image of a cross-section ~ 20 to 30 µm ahead of the reaction front (same as location 2 in Fig. 1(c)). The white dashed-line in (a) is a visual aid for the reaction front while the rectangular box on the right side of (a) is an artifact resulting from a previous SEM raster over the region. A grain boundary with Pu_6Fe is observable from the lower left, through the cross section to the upper right. (b) Higher magnification of this cross sectional image shows partial corrosion advancing into this grain from the grain boundary where Pu_6Fe was coincidentally detected.

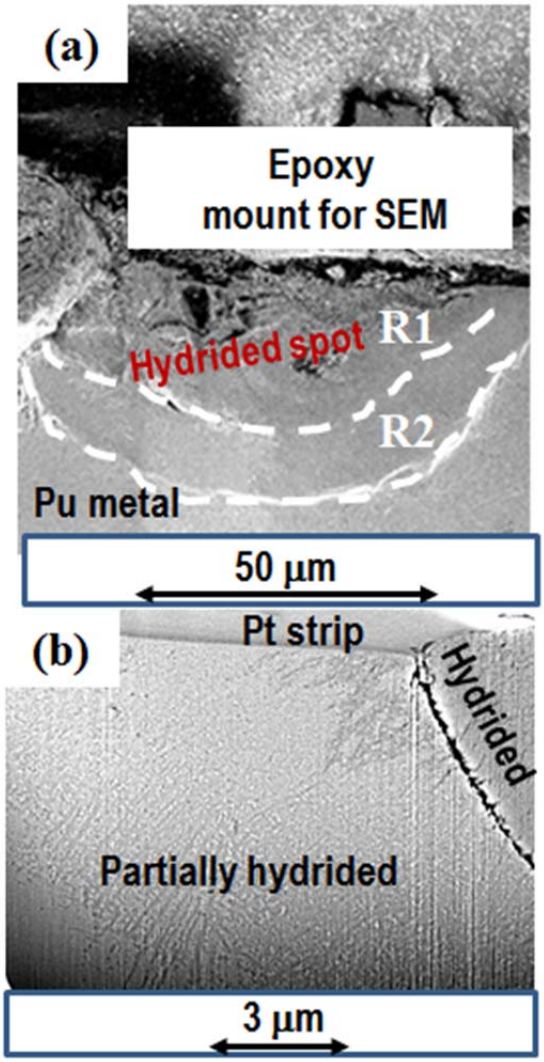

Fig. (4): FIB-SEM images showing the existence of partial hydriding ahead of the reaction front. The two hand-drawn dashed lines labeled R1 and R2 indicate the extents of hydrided and partially hydrided regions. (b) is a higher magnification of (a) near the boundary between the fully and partially hydrided regions.

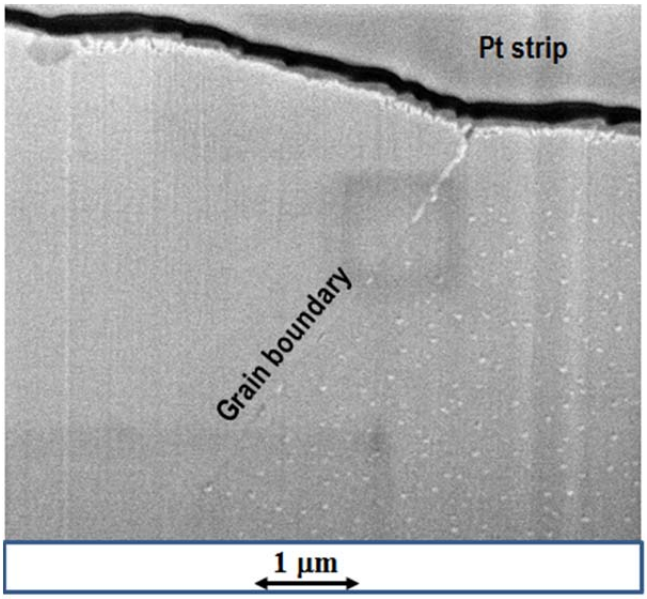

Fig. 5: FIB-SEM image of metal grains ~ 100 µm ahead of the apparent reaction front. No apparent hydriding was found on either side of this grain boundary which is a few grains ahead of the reaction front (location "3" in Fig. 1(c)).